J. Plasma Phys. (2016), *vol.* 82, 595820502
doi:10.1017/S0022377816000829

Electrostatic particle-in-cell simulation of heat flux mitigation using magnetic fields

Karl Felix Lüskow[1,†], S. Kemnitz[1,2], G. Bandelow[1], J. Duras[1,3], D. Kahnfeld[1], P. Matthias[1], R. Schneider[1] and D. Konigorski[4]

[1]Institute for Physics, Ernst-Moritz-Arndt University of Greifswald, Felix-Hausdorff-Str. 6, D-17489 Greifswald, Germany

[2]Institute of Computer Science, University of Rostock, Albert-Einstein-Str. 22, D-18059 Rostock, Germany

[3]Department of Applied Mathematics, Physics and Humanities, Nürnberger Institute of Technology, Keßlerplatz 12, D-90489 Nürnberg, Germany

[4]Airbus Operations GmbH, Emerging Technologies and Concepts, Kreetslag 10, D-21129 Hamburg, Germany

(Received 13 June 2016; revised 1 September 2016; accepted 2 September 2016)

The particle-in-cell (PIC) method was used to simulate heat flux mitigation experiments with partially ionised argon. The experiments demonstrate the possibility of reducing heat flux towards a target using magnetic fields. Modelling using the PIC method is able to reproduce the heat flux mitigation qualitatively. This is driven by modified electron transport. Electrons are magnetised and react directly to the external magnetic field. In addition, an increase of radial turbulent transport is also needed to explain the experimental observations in the model. Close to the target an increase of electron density is created. Due to quasi-neutrality, ions follow the electrons. Charge exchange collisions couple the dynamics of the neutrals to the ions and reduce the flow velocity of neutrals by radial momentum transport and subsequent losses. By this, the dominant heat-transport channel by neutrals gets reduced and a reduction of the heat deposition, similar to the experiment, is observed. Using the simulation a diagnostic module for optical emission is developed and its results are compared with spectroscopic measurements and photos from the experiment. The results of this study are in good agreement with the experiment. Experimental observations such as a shrank bright emission region close to the nozzle exit, an additional emission in front of the target and an overall change in colour to red are reproduced by the simulation.

Key words: magnetized plasmas, plasma dynamics, plasma simulation

1. Introduction and experimental overview

The thermal protection system of spacecrafts is one of the most expensive parts for space missions. Large efforts are undertaken to develop and use special materials for the thermal protection system (Blosser 1996). One idea was to use magnetic fields

† Email address for correspondence: lueskow@physik.uni-greifswald.de

for heat flux reduction. If it is possible to reduce the heat flux by externally applied electromagnetic fields, one would be able to use simpler and cheaper materials. In 2002 the European Space Agency (ESA) started an investigation of heat flux mitigation by means of MHD (magnetohydrodynamics) in partially ionised argon (Gülhan *et al.* 2009). Argon was chosen as test gas for this campaign due to its chemical inertness. This simplifies the analysis and makes the inclusion of complicated plasma chemistry unnecessary.

In the experiment an arc jet was used to create a flow field, with a typical Mach number between 5 and 10, which hits a target. The heat flux on the target surface was measured with and without a magnetic field. Applying a dipole-like external magnetic field a strong heat flux mitigation was observed (Gülhan *et al.* 2009). However, even up to now, the experiments could not be reproduced by models based on Navier–Stokes fluid codes for neutrals with fluid models for the plasma components. One was not able to explain the main effects leading to the heat flux reduction.

One major problem for the modelling is the lack of information about the plasma component in the experiment. There exist only average values for density ($n_e \approx 10^{11}\,\mathrm{cm}^{-3}$) and temperature ($T_e \approx 0.7$ eV), whereas the neutral component is well characterised using different diagnostic methods in terms of temperature and velocities, including axial and radial profiles at specific locations. The average neutral density n_n is $\approx 10^{15}\,\mathrm{cm}^{-3}$.

In addition, spectroscopic data and a video from the experiment are available (Detlev Konigorski, personal communications, January 2014). During the experiment a clear change in the emission was visible in photos looking into the vacuum chamber onto the blunt body. The flow illumination changed to a red colour when the magnetic field was applied, confirmed in observations by Kranc, Cambel & Yuen (1969) in a similar experiment. The large bright area between the arc jet exit and the target shrank by activating the magnetic field and a small bright spot directly in front of the centre of the target appeared (see figure 6 of Gülhan *et al.* (2009)).

There are several groups that have tried to reproduce the experiment in simulations. They all applied Navier–Stokes codes or direct simulation Monte Carlo codes for the neutral gas description. In contrast to the complex and rather complete models of neutral transport, only fluid models for the description of the plasma were used, mostly with estimated transport coefficients (Katsurayama *et al.* 2008; Otsu *et al.* 2012).

Using a self-consistent kinetic particle method instead of fluid models a more realistic description of neutral and plasma dynamics and their interaction is possible. Specifically, an existing particle-in-cell (PIC) code with Monte-Carlo collisions (Tskhakaya *et al.* 2007) is used for this study.

Perturbed plasma source distribution functions are typical for plasma sources, e.g. those shown by Godyak & Piejak (1990) for RF (radio frequency) discharges or by Behringer & Fantz (1994) for DC (direct current) discharges. Such non-Maxwellian characteristics of the plasma components are also expected from the arc jet.

2. Simulation method

The well-established PIC method is combined with Monte Carlo collisions (PIC-MCC). In plasma physics, the PIC method is a widely accepted method to obtain a better understanding of the basic physical mechanisms of various systems because the PIC-MCC approach provides full insight into all (microscopic and macroscopic) parameters. A more detailed description of the PIC-MCC method itself can be found in several reviews (Birdsall & Langdon 2004; Tskhakaya *et al.* 2007)

https://doi.org/10.1017/S0022377816000829 Published online by Cambridge University Press

The principle of PIC is to follow so-called super-particles. Each of these represents the same number of physical particles following the same trajectory as single particles due to their identical mass-to-charge ratio, resulting in the same Lorentz force. The electric field for the Lorentz force is calculated self-consistently on a spatially equidistant grid from the Poisson equation. In the electrostatic approximation, magnetic field effects are included in the Lorentz force, but are determined just by their external sources (e.g. magnets). Corrections from plasma currents are neglected. Particles experience collisions according to Monte Carlo collision algorithms. This allows one to implement all relevant collision types. For this work electron–neutral elastic, ionisation, excitation, Coulomb collision, neutral–neutral and charge exchange collisions are implemented. Effective ionisation and radiation energy losses are included in the model. Neutrals are treated as plasma particles with zero charge. Technically, this is identical to a DSMC (direct simulation Monte Carlo) model for the neutrals.

In the experiment, the neutral density is approximately four orders of magnitude larger than the electron density (Gülhan *et al.* 2009). If one uses the same super-particle factor for plasma and for neutrals, one runs into computational memory limits due to the large number of neutral particles.

Due to the relatively low electron energy compared with ionisation energies above 15 eV, there are only a very small number of ionisation collisions. Due to the very low ionisation degree, the neutrals can be assumed to be practically decoupled in density from the plasma component.

Therefore, different weights for neutrals and plasma particles are taken care of by scaling the cross-section of collisions with neutrals linearly. The cross-section for neutral–neutral collisions is increased quadratically by this factor. These scalings are technically equivalent to modifying the super-particle factor for neutrals. This allows one to reduce the number of pseudo-particles for neutrals to a moderate number. In this work a scaling factor of 10^3 is used.

The spatial domain is two-dimensional (axial and radial). Due to collisions three components in velocity space need to be resolved. The domain consists of 400 axial and 140 radial cells. With a cell size of $\Delta r \approx 1.05$ mm this leads to a domain of 42 cm $\times$ 14 cm. The cell size and the time step $\Delta t \approx 10^{-12}$ s are chosen in order to resolve the Debye lengths and the electron cyclotron frequency. For this system the cyclotron frequency ($\nu \approx 7 \times 10^{10}$ Hz) in the region with strong magnetic fields is higher than the plasma frequency ($\omega_{p,e} \approx 3 \times 10^{10}$ Hz).

The target is placed directly at the symmetry axis at the right side of the domain. It has a radius of 3.6 cm and its surface is located at 26 cm according to the experimental conditions. The target has a dielectric surface made out of quartz ($\epsilon = 4.27$) and the inner part is metallic. All boundaries except the left one have a fixed potential of zero. The left domain boundary is set to 0.5 V, to represent the exit of the arc jet and ensure that particles move towards the target. At outer domain boundaries all particles are absorbed. Plasma particles that hit the target are also absorbed, only neutrals are reflected at the surface of the target. This represents the inertness against chemical reactions of the noble gas argon.

The size of the domain is scaled down by a factor of 100 to overcome spatial resolution limits. One applies a self-similarity scaling keeping the relevant non-dimensional parameters constant, namely the ratio of system length to gyroradii and to mean free path. The first represents the influence of the magnetisation by the external magnetic field, the second the collisional effects. By increasing all densities and the magnetic field by the same factor, the ratio of system length to gyroradii

https://doi.org/10.1017/S0022377816000829 Published online by Cambridge University Press

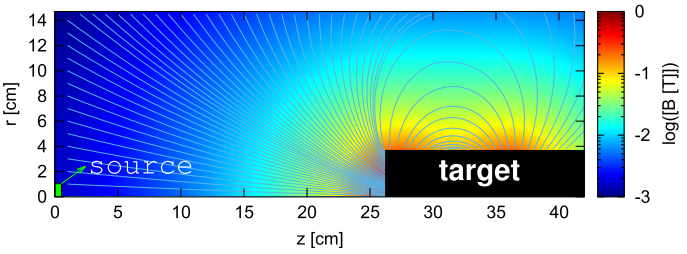

FIGURE 1. Magnetic field in the simulation domain.

and to mean free path is conserved. This ensures the physical correctness of the simulation as proven by Taccogna *et al.* (2005).

The external magnetic field was calculated using the finite-element magnetic method solver (FEMM) (Meeker 2010). The topology of the dipole-like magnetic field is shown in figure 1.

For neutrals a uniform background density (representing background pressure effects) is combined with the main particle source at the left side of the domain near the axis with a radial extension up to 1 cm. The location of the source is shown in green in figure 1. Neutrals are injected with a Maxwellian-distributed velocity with a drift of 2070 m s^{-1} in axial direction according to the mean velocity measured by microwave interferometry. For every sampled velocity it is ensured that particles leave the source with an initial angle smaller than 12° to reproduce the angular distribution of the particle source in the experiment. The characterisation of the plasma species coming from the arc jet is not known experimentally. Therefore, variation of the source parameters was used to represent the experiment as well as possible. Finally, the following plasma source distributions were used. Ions have similar source distributions as the neutrals.

Electrons are injected with a two-Maxwellian distribution. The first one has a shift in energy of approximately 1 eV to represent the measured averaged temperature from experiment and a width of 1 eV. A second Maxwellian with the same shift and variable width and source strength is added. The parameters are fitted to get as close as possible to the experimental results without a magnetic field. The best result are obtained for a source strength of 1/3 of the bulk source and a width of 20 eV. The second contribution is necessary to provide some electrons with higher energies of above 13 eV, otherwise there is no line emission in the visible range as observed in the photos and in the spectroscopic analysis of the experiment. According to Kranc *et al.* (1969) the red emission is due to excitation of metastable argon atoms with energies of approximately 11 eV. The resulting electron energy distribution function is shown in figure 2 for different axial positions.

The number of injected particles is chosen to approximate the average density for electrons ($n_e = n_i \approx 2.8 \times 10^{11}$ cm^{-3}) and for neutrals ($n_n \approx 1.6 \times 10^{15}$ cm^{-3}). For a typical run approximately 4×10^6 super-particles for each plasma species and 6×10^6 super-particles for neutrals are used.

During the experiment strong fluctuations were observed when the magnetic field was applied. To reflect this observation in the model in the case of an applied magnetic field, radial anomalous diffusion is implemented. In addition to the Bohm diffusion (Bohm *et al.* 1949), which scales like

$$D \propto \frac{T}{B}, \tag{2.1}$$

https://doi.org/10.1017/S0022377816000829 Published online by Cambridge University Press

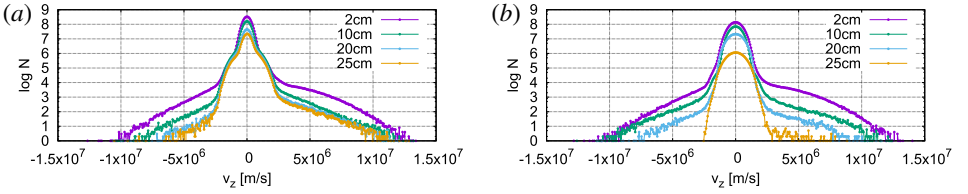

FIGURE 2. Electron axial velocity distribution functions for different axial positions averaged over 10^5 time steps ((*a*): without magnetic field, (*b*) with magnetic field).

with the temperature T and the magnetic field B, a constant transport is taken into account. This contribution is motivated by the fact that the arc jet itself delivers a turbulent flow due to angular gas insertion. Movies of the experiment give the impression that this turbulence is strongly increased within the source by the activation of the magnetic field. For cylindrical geometry the radial diffusion has to be implemented correctly as derived by Bormann, Brosens & De Schutter (2001):

$$p_{\pm}^{r} = \frac{1}{2}\left(1 \pm \frac{1}{2k}\right), \tag{2.2}$$

with $k = r/\sqrt{2D \times \Delta t}$ for a diffusion coefficient D. The diffusion coefficient is set to 10 m^2 s^{-1} for plasma particles and 1 m^2 s^{-1} for neutrals. The estimation for the coefficients is based on diffusion coefficients from magnetic fusion (Perkins *et al.* 1994). Bohm *et al.* (1949) showed that turbulence in a plasma can be created or at least be enhanced by magnetic fields. The non-local effect is also observed in systems like the cylindrical Hall thruster from PPPL (Princeton Plasma Physics Laboratory) (Ellison, Raitses & Fisch 2012).

3. Discussion

The most important finding from the experiment was a strong heat flux mitigation by activating the magnetic field. According to Gülhan *et al.* (2009) the total heat flux was reduced by 85 %. Due to the large difference between plasma density and neutral density one can expect that most of the heat flux is carried by neutrals. Up to now it has not been understood why their fluxes could be affected so strongly by a magnetic field, because neutrals experience no direct force from the Lorentz force. This is only possible if it is induced by the interaction with the plasma components which react to magnetic fields.

3.1. *Heat flux mitigation*

In the PIC simulation a heat flux mitigation is observed for the case when the magnetic field is applied. This effect is created by a combination of radial turbulent transport and kinetic effects. The first is introduced parametrically the latter is treated self-consistently. The neutral flux is reduced indirectly. Electrons follow the magnetic field lines guiding them towards the target and build up a region of higher density in front of the target. Ions follow due to the constraint of quasi-neutrality. If neutrals arrive in this region their velocity gets reduced by charge exchange collisions with slower ions. The charge exchange collisions act as a parallel momentum sink for the neutrals slowing them down (Lüskow *et al.* 2016). Neutrals lose energy and momentum due to the increased number of collisions with plasma particles and by

https://doi.org/10.1017/S0022377816000829 Published online by Cambridge University Press

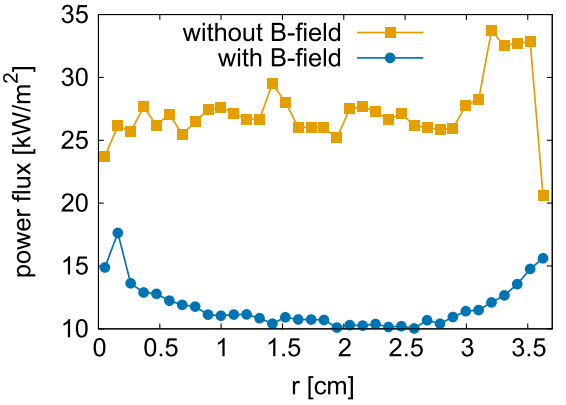

FIGURE 3. Simulated radial profile of the total target heat flux.

this the neutral energy flux to the target is reduced. In charge exchange collisions momentum and energy are transferred from neutrals to ions. Due to strong radial transport most of the ions are guided away from the target in the radial direction and the heat flux of ions is only weakly increased. The reduction of total heat flux is shown in figure 3. The integral total heat flux is reduced by 58% compared to the case without a magnetic field, representing very well the experiment. Details of the model do not yet fit and require further adjustment in terms of source definitions and transport. For example, the strong reduction of the heat flux in the centre is not well represented. Further experimental characterisation of the plasma components and the neutrals in the case with a magnetic field would be very helpful to guide this process.

3.2. *Optical emission spectral analysis*

Experiments used mostly spectroscopy and photos to study the overall behaviour of the system when applying magnetic fields. To verify the simulation against the experiment, diagnostic routines in the PIC-MCC model are developed that provide the emission spectrum for every cell. In the Monte Carlo collision routines, effective energy losses are taken into account. In the open-ADAS library (Summers 1994; Summers & O'Mullaine 2011) one obtains photon emissivity coefficients (PEC) for many transition lines of argon, both ionic and atomic. Details about the calculation of open-ADAS' PECs for argon are given in O'Mullane (2008). The PECs are effective coefficients from a collisional radiative model and are functions of electron energy and density. Due to the kinetic character of PIC, it is possible to calculate the energy distribution function in every cell of the domain. A diagnostics module is added to the code, in which for each wavelength an intensity is calculated integrating the PECs with respective densities and temperatures of electrons over the time-averaged distribution function. By this, for each cell, an emission spectrum can be reconstructed.

For a more detailed comparison with spectroscopic measurements two cells are chosen. The first one is within the shock layer in front of the target ($r = 1\Delta r$, $z = 220\Delta r$), the other one is located in the free stream region ($r = 60\Delta r$, $z = 90\Delta r$). For both regions spectroscopic measurements exist. For all spectra, intensities are scaled to a maximum intensity. This was chosen to represent a typical value for

https://doi.org/10.1017/S0022377816000829 Published online by Cambridge University Press

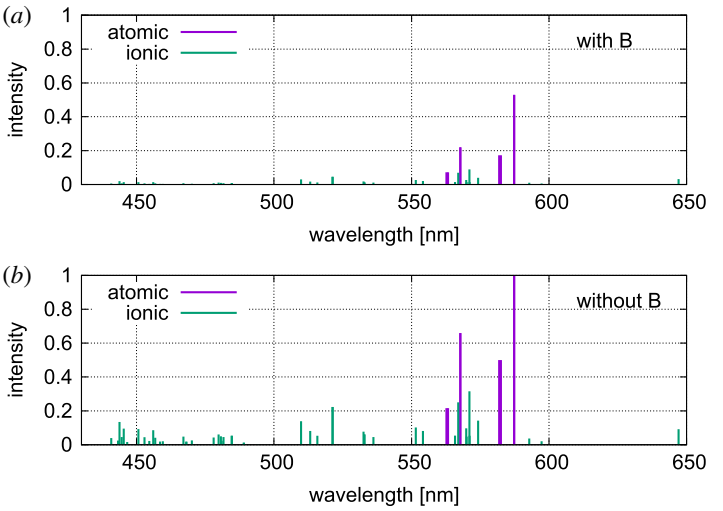

FIGURE 4. Optical emission spectra in the free stream region, (*a*) with magnetic field and (*b*) without magnetic field.

over-saturation of the detector chips in the CCD (charge-coupled device) camera (Janesick 2001). Details will be discussed later. In the free stream, a loss of intensity in several emission lines is visible in figure 4 with the applied magnetic field. This is in good agreement with emission spectroscopy.

Overall, the emission pulls back from the target. This is a consequence of the changes in the electron density distribution. The electrons follow the magnetic field lines and are guided back towards the exit and upwards by the dipole-like field acting similar to a magnetic cusp mirror. Consequently, the electron density is reduced as the magnetic field is applied compared to the non-magnetised case. Therefore, the chance for excitation is also reduced and the overall emission rate is decreased. In the shock the situation is quite different. Experimentally, there is a small bright spot in front of the centre of the target which appears when activating the magnetic field. Here, an increase of intensity of several emission lines is observed (figure 7 of Gülhan *et al.* (2009)). The same tendency appears in our model for this region. Calculated optical emission spectra are shown in figure 5 with and without a magnetic field.

In the experiment the whole photo turns more red by switching on the magnetic field. This is represented in the simulation by larger peaks in the red wavelength region in the cells around the target.

Each wavelength in the optical spectrum has a specific colour. Therefore, it is possible to use the spectrum for every cell in order to calculate a colour, represented by a RGB (red-green-blue)-value. With this, one can try to create a simulated photo that can be compared to the experiment. Details about this procedure will be published elsewhere. CCD cameras have a so-called full-well capacity that describes the maximum number of charges that can be saved in one pixel (Janesick 2001). If this number is reached the CCD sensor for this pixel is saturated and the cell is plotted in white in figure 6, indicating a bright region of emission in the experimental photo. Black regions are cells with no emission.

On the left side the original colour data are plotted. On the right there is a zoom into the shock region in front of the target, shifted in colour space towards green to visualise clearer the effects at the shock.

https://doi.org/10.1017/S0022377816000829 Published online by Cambridge University Press

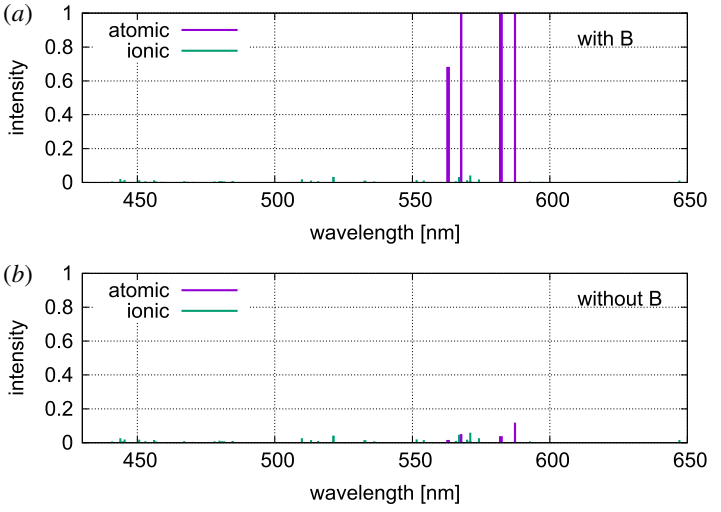

FIGURE 5. Optical emission spectra in the shock front region, (*a*) with magnetic field and (*b*) without magnetic field.

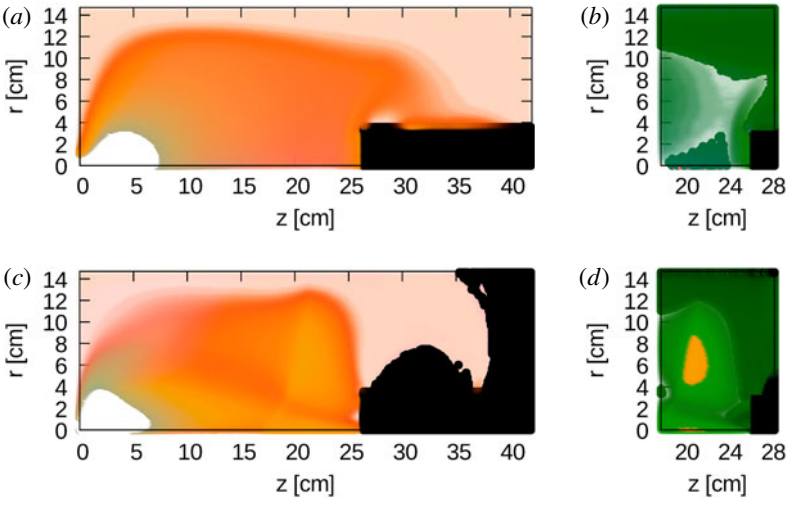

FIGURE 6. (*a*,*c*) colour plot of the optical emission, (*b*,*d*): zoom into the shock region with shifted colours ((*a*,*b*) without magnetic field, (*c*,*d*) with magnetic field).

One can see several features from the experiment which are in good agreement with the simulation. The white area with saturated cells has shrunk towards the arc jet exit when the magnetic field is applied. The shock is smeared out and there are additional emission regions directly in front of the target, one at the centre and one at an outer radial position.

https://doi.org/10.1017/S0022377816000829 Published online by Cambridge University Press

4. Conclusions

A PIC-MCC code was modified and applied to a heat flux mitigation experimental campaign performed by ESA in 2007. During the campaign it was shown that heat flux towards a target can be reduced by a external magnetic field.

The simulation reproduces the heat flux reduction qualitatively. The magnetic field leads to a change in electron and ion density by affecting the trajectories of the charged particles through the Lorentz force. Magnetic field lines in the dipole-like field converge to the centre of the target. As particles are guided into this region a shield of high plasma density builds up in front of the target. Neutral transport is affected by charge exchange collisions with ions acting as a momentum sink for the neutrals and reducing the neutral axial velocity. By this, the resulting total neutral heat flux is reduced. Ion heat flux is increased only weakly, because the radial losses due to the magnetic field and turbulence get stronger.

In addition, the simulation was verified against experimental spectroscopy using optical emission analysis. In the free stream region a loss of intensity for all wavelengths appeared, whereas in front of the target an increase of the intensity is observed. Both effects were in good agreement with the experiment.

A photo was simulated from the calculated optical emission spectrum. The simulation reproduces the observed optical effects when applying the external magnetic field. These effects are an overall red shift, a smaller bright emission region close to the arc jet exit and an emission region in front of the target.

Acknowledgements

This work was supported by the German Space Agency DLR through Project 50RS1508.

REFERENCES

BEHRINGER, K. & FANTZ, U. 1994 Spectroscopic diagnostics of glow discharge plasmas with non-maxwellian electron energy distributions. *J. Phys.* D **27** (10), 2128–2135.

BIRDSALL, C. K. & LANGDON, A. B. 2004 *Plasma Physics via Computer Simulation*. CRC Press.

BLOSSER, M. L. 1996 Advanced metallic thermal protection systems for reusable launch vehicles. NASA Technical Memorandum 110296, October 1996.

BOHM, D., BURHOP, E. H. S., MASSEY, H. S. W. & WILLIAMS, R. W. 1949 The characteristics of electrical discharges in magnetic fields. In *National Nuclear Energy Series: Electromagnetic Separation Project 6*, McGraw-Hill.

BORMANN, G., BROSENS, F. & DE SCHUTTER, E. 2001 Modeling molecular diffusion. In *Computational Methods in Molecular and Cellular Biology: from Genotype to Phenotype*, pp. 189–224. MIT Press.

ELLISON, C. L., RAITSES, Y. & FISCH, N. J. 2012 Cross-field electron transport induced by a rotating spoke in a cylindrical hall thruster. *Phys. Plasmas* **19** (1), 013503.

GODYAK, V. A. & PIEJAK, R. B. 1990 Abnormally low electron energy and heating-mode transition in a low-pressure argon rf discharge at 13.56 mHz. *Phys. Rev. Lett.* **65** (8), 996.

GÜLHAN, A., ESSER, B., KOCH, U., SIEBE, F., RIEHMER, J., GIORDANO, D. & KONIGORSKI, D. 2009 Experimental verification of heat-flux mitigation by electromagnetic fields in partially-ionized-argon flows. *J. Spacecr. Rockets* **46** (2), 274–283.

JANESICK, J. R. 2001 *Scientific Charge-coupled Devices*, vol. 117. SPIE Press.

KATSURAYAMA, H., KAWAMURA, M., MATSUDA, A. & ABE, T. 2008 Kinetic and continuum simulations of electromagnetic control of a simulated reentry flow. *J. Spacecr. Rockets* **45** (2), 248–254.

KRANC, S., CAMBEL, A. B. & YUEN, M. C. 1969 *Experimental Investigation of Magnetoaerodynamic Flow Around Blunt Bodies*, vol. 1393. National Aeronautics and Space Administration.

LÜSKOW, K. F., KEMNITZ, S., BANDELOW, J., DURAS, J., KAHNFELD, D., SCHNEIDER, R. & KONIGORSKI, D. 2016 Particle-in-cell simulation concerning heat-flux mitigation using electromagnetic fields. *Plasma Phys. Technol.* (submitted).

MEEKER, D. 2010 Finite element method magnetics. *FEMM* **4**, 32.

O'MULLANE, M. 2008. Photon emissivities for ArI and ArII. ADAS Communications: ADAS C(08)-01.

OTSU, H., KATSURAYAMA, H., KONIGORSKI, D. & ABE, T. 2012 Effect of the strong magnetic field on the electrodynamic heat shield system for reentry vehicles. *In 43rd AIAA Plasmadynamics and Lasers Conference*. p. 2731. American Institute of Aeronautics and Astronautics.

PERKINS, F., BARABASCHI, P., BOUCHER, D., CORDEY, J. G., COSTLEY, A., DEBOO, J., DIAMOND, P. H., FUJISAWA, N., GREENFIELD, C. M., HOGAN, J. *et al.* 1994 Iter physics basis. In *Plasma Physics and Controlled Nuclear Fusion Research: Proceedings of the International Conference on Plasma Physics and Controlled Nuclear Fusion Research*, vol. 15, p. 477. International Atomic Energy Agency.

SUMMERS, H. P. & O'MULLAINE, M. 2011 Atomic data and modelling for fusion: the adas project. In *7th International Conference on Atomic and Molecular Data and THEIR Aplications-ICAMDATA-2010*, vol. 1344, pp. 179–187. AIP Publishing.

SUMMERS, H. P. 1994 Atomic data and analysis structure. *JET Rep*.

TACCOGNA, F., LONGO, S., CAPITELLI, M. & SCHNEIDER, R. 2005 Self-similarity in hall plasma discharges: applications to particle models. *Phys. Plasmas* **12** (5), 053502.

TSKHAKAYA, D., MATYASH, K., SCHNEIDER, R. & TACCOGNA, F. 2007 The particle-in-cell method. *Contrib. Plasma Phys.* **47** (8–9), 563–594.